ACSNANO www.acsnano.org

ARTICLE

Collective Molecular Mechanisms in the $CH_3NH_3PbI_3$ Dissolution by Liquid Water

Claudia Caddeo,*[,†] Maria Ilenia Saba,[†] Simone Meloni,[‡] Alessio Filippetti,[†,§] and Alessandro Mattoni*[,†]

[†]Istituto Officina dei Materiali (CNR - IOM) Cagliari, Cittadella Universitaria, I-09042 Monserrato (Ca), Italy
[‡]Department of Mechanical and Aerospace Engineering, Università La Sapienza, Via Eudossiana 18, 00184 Roma, Italy
[§]Dipartimento di Fisica, Università degli Studi di Cagliari, Cittadella Universitaria, I-09042 Monserrato (Ca), Italy

Supporting Information

ABSTRACT: The origin of the dissolution of methylammonium lead trihalide (MAPI) crystals in liquid water is clarified by finite-temperature molecular dynamics by developing a MYP-based force field (MYP1) for water−MAPI systems. A thermally activated process is found with an energy barrier of 0.36 eV consisting of a layer-by-layer degradation with generation of inorganic PbI_2 films and solvation of MA and I ions. We rationalize the effect of water on MAPI by identifying a transition from a reversible absorption and diffusion in the presence of vapor to the irreversible destruction of the crystal lattice in liquid due to a cooperative action of water molecules. A strong water−MAPI interaction is found with a binding energy of 0.41 eV/H_2O and wetting energy of 0.23 N/m. The water vapor absorption is energetically favored (0.29 eV/H_2O), and the infiltrated molecules can migrate within the crystal with a diffusion coefficient $D = 1.7 \times 10^{-8}$ cm^2/s and activation energy of 0.28 eV.

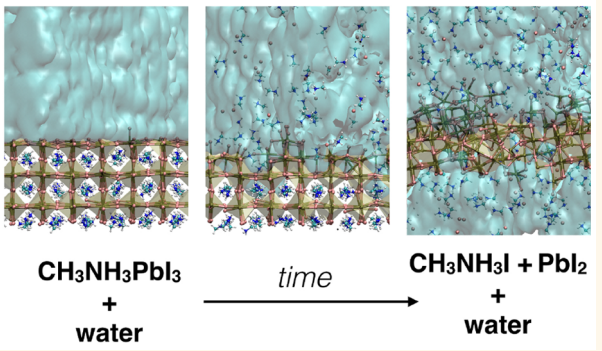

KEYWORDS: *hybrid perovskites, classical molecular dynamics, MYP, model potential, DFT, degradation kinetics, water adhesion*

The importance of hybrid organic−inorganic perovskites has greatly increased in recent years due to the exceptional photovoltaic properties of methylammonium lead trihalide, $CH_3NH_3PbI_3$ (MAPI), that make it of great promise for low-cost, solution-processable hybrid solar cells. This material with a perovskite crystalline structure[1] has light absorption and charge transport properties comparable to those of the most efficient inorganic semiconductors,[2−4] making it possible to manufacture 22% efficient MAPI solar cells.[5−7] The importance of MAPI extends far beyond photovoltaics with many possible applications ranging from optoelectronics[8,9] and lasing,[10−12] to photocatalysis[13] and thermoelectricity.[14−16]

Despite its excellent optoelectronic properties, MAPI has drawbacks such as thermal instability at relatively low temperatures.[17−19] More importantly the material easy degrades in the presence of highly polar solvents, such as water.[20] Since solar cells operate at ambient conditions, the presence of water in air can easily induce the degradation of MAPI devices, also raising concerns on the dispersion of toxic lead in the environment.

Although it is in principle possible to protect the active layer by encapsulation,[21−29] waterproofing the material,[30−33] and to improve the stability by mixed-cation systems,[34] a conclusive solution to the problem has not been achieved so far. The understanding of the water−MAPI interaction and of the irreversible degradation mechanisms of hybrid perovskites is accordingly a key issue toward the development of usable devices.

Several experimental works have reported the effects of the exposure of MAPI to humidity: for example, Leguy *et al.*[35] have observed that when MAPI single crystals and thin films are exposed to water vapor at room temperature, hydrated crystal phases are formed. Notably such transformation can be reversed upon drying. Water absorption under vapor exposure is not well understood. Müller *et al.*[36] have observed water penetration into MAPI thin films within seconds at low, 10% humidity, while Zhu *et al.*[37] did not observe infiltration up to 80% relative humidity. Most works agree that water infiltration is surface-originating, and defects or grain boundaries can enhance the process. Despite the different results, all experiments indicate that MAPI transformations under vapor conditions have a reversible character.

The exposure to liquid water instead always gives rise to irreversible dissolution of MAPI with the formation of PbI_2.

Received: June 13, 2017
Accepted: August 7, 2017
Published: August 7, 2017

DOI: 10.1021/acsnano.7b04116
ACS Nano XXXX, XXX, XXX−XXX

Degradation is very effective in this condition, and it is observed already for very small amounts of liquid, such as condensed drops on a thin film surface, or for fast dipping in water.[35,38] Degradation has been proposed to proceed through the loss of $CH_3NH_3^+$ (with I^- as the counterion) and the irreversible formation of the reaction product PbI_2.

Water also has an effect on the thermal degradation of MAPI at high temperature. In the presence of humid air the kinetics is faster and characterized by a lower activation energy (0.96 eV in air *versus* 1.54 eV *in vacuo*).[39]

The molecular origin of dissolution has been searched by *ab initio* atomistic simulations. The studies of water on MAPI surfaces have been performed considering two possible cases: MAI- or PbI_2-terminated surfaces. In the former case, *i.e.*, the less stable MAI surface, it has been demonstrated that vapor and liquid water infiltration[40−43] are highly favored. Furthermore, by using Car−Parrinello molecular dynamics (CPMD),[44] Mosconi *et al.*[42] observed the solvation of a MAI unit detached from this surface in liquid water.

Conversely, the interaction of water with the PbI_2-terminated surface has slower dynamics far from reach for *ab initio*. In fact the full degradation of the PbI_2-terminated surface of MAPI[42] has never been observed, even in the presence of liquid water. The computational cost of CPMD limits the time scale to a few tens of picoseconds, which is in any case too short to observe degradation of the PbI_2-terminated MAPI surface and to clarify the infiltration mechanism under controlled thermodynamic conditions. Accordingly, the molecular origin and the critical conditions for the overall MAPI dissolution in liquid water are still unexplored and require alternative approaches.

Recently, a few model potentials have been reported for the study of MAPI over longer time and length scales by classical molecular dynamics.[45−47] In particular, the MYP0 potential[45] has demonstrated to reproduce several relevant properties of MAPI, such as orthorhombic-to-tetragonal transition, vibrational properties,[48] defect diffusion,[49] thermal transport properties,[50,51] and the coexistence of ordered and disordered molecular domains in MAPI under specific thermal treatments.[52] To date, the only study of water−MAPI systems by model potential molecular dynamics (MPMD) has been performed by Gutierrez-Sevillano *et al.*[53−55] In their paper the authors have adopted a force field that describes the MAPI precursors in solvent but that is not able to reproduce the properties of the crystalline phase of MAPI. Here we want to simulate the dissolution process that, according to literature, involves the formation of PbI_2 in liquid water; thus we need a force field able to model both the crystal and its dissolved components.

In this work we refine and extend the MYP0 force field to treat MAPI−water interactions and we study the full process of dissolution of MAPI crystals in water by finite-temperature molecular dynamics. We are able to clarify the transition from reversible phenomena (such as vapor infiltration) to dissolution in liquid water. The kinetics reveals an Arrhenius behavior with an activation energy of 0.36 eV. Such an activation energy derives from a collective mechanism involving clusters of water molecules inducing the dissolution into ionic components. This decomposition process is fast and efficient in water, and it represents a first step toward a slower irreversible degradation involving higher energy reactions, ∼1 eV,[39,56] such as deprotonation of methylammonium into methylammine[39] or methylammonium fragmentation into ammonia and CH_3I.[56,57]

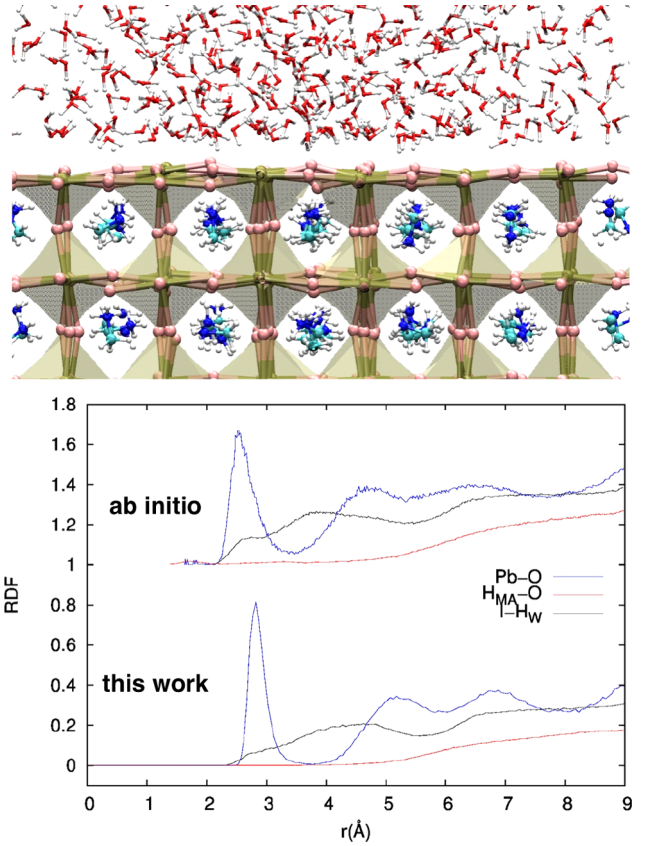

Figure 1. (Top) Snapshot of the simulated interface between the PbI_2-terminated perovskite slab and the water layer. Red is O, white is H, pink is I, dark gold is Pb, cyan is C, and blue is N. Polyhedra are made by triangles that connect all triplets of groups of atoms within a 4 Å radius. (Bottom) I−H_W (black), H_{MA}-O (red), and Pb−O (blue) radial distribution functions (RDFs) at the interface, averaged over the first 25 ps. The top curves are shifted to enhance visibility and correspond to the *ab initio* RDFs of ref 42.

RESULTS AND DISCUSSION

System under Study. The typical system studied in this work consists of water molecules (either a single molecule, a cluster, or a liquid layer) on top of a (001) PbI_2-terminated MAPI slab (see Figure 2). The choice of this surface stems from the fact that the (001) is one of the lowest energy cuts for

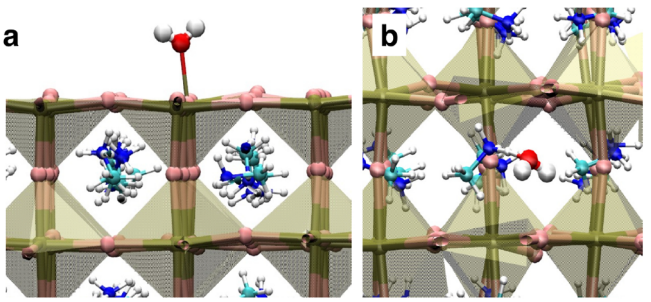

Figure 2. (a) Water molecule bound to the PbI_2-terminated perovskite slab showing the formation of the Pb−O bond; (b) water molecule infiltrated within the MAPI crystal showing the formation of the H−O link between the methylammonium and water. Both snapshots are taken during dynamics at room temperature. Red is O, white is H, pink is I, dark gold is Pb, cyan is C, and blue is N.

DOI: 10.1021/acsnano.7b04116
ACS Nano XXXX, XXX, XXX−XXX

MAPI.[58] Furthermore, the PbI_2 termination is interesting for applications since its surface states can act as intermediate levels for hole transfer.[59] Additional calculations for the MAI-terminated surface were performed to validate results on degradation (see the Supporting Information).

The MAPI crystal is periodically replicated in the $x-y$ directions and the lateral sizes are $L_x = 3.6$ nm × $L_y = 3.4$ nm. The slab is 1.8 nm thick along the z direction. For the study of vapor only one water molecule is put on the MAPI surface, corresponding to a surface density of 2.4×10^{-10} g/cm^2, while for the liquid case, a 2.5 nm thick layer of water molecules is relaxed on top of the surface (surface density of $\sim 8 \times 10^{-8}$ g/cm^2). Overall up to 10^4 atoms were used in the simulations.

MAPI interatomic forces are described by a refined version of the MYP0 model potential[45] (referred to as MYP1). The main difference is a reduction of the Pb and I charges and the use of PbI Buckhingham parameters close to the potential of Winkler *et al.*,[60] as interestingly suggested by Handley *et al.*[61] With respect to the Handley potential, the MYP1 is still able to reproduce the orthorhombic-to-tetragonal transition. An extensive validation of the model against density functional theory (DFT) and experimental data can be found in the Supporting Information.

The TIP3P model[62] is used for water. This is a simple three-site model for water with a low computational cost, and it is widely adopted in the literature for a broad range of systems and problems. The MAPI−water interactions are described as the sum of Coulomb and Lennard-Jones (12-6) contributions and are fitted on *ab initio* results for structure and energetics of suitable water−MAPI systems (see Supporting Information). In addition the present model is able to reproduce the water/MAPI radial pair distribution functions (see Figure 2), the easiness of water penetration inside the MAPI surface, and the experimentally observed insolubility of PbI_2 in water[35,36] (see Supporting Information).

Vapor Phase Analysis. First, we want to quantify the absorption of water on the MAPI surface and its ability to infiltrate inside the MAPI crystal. Near saturation, a parcel of air contains ∼28 g of water per cubic meter at room temperature and pressure, which corresponds to one water molecule per 10^3 nm^3. With reference to our model, vapor phase conditions are thus attained by placing a single water molecule on the surface.

A single water put in front of the surface is attracted by the crystal, and its oxygen eventually binds to a Pb atom on the surface, giving rise to a polar Pb−O link. This is in agreement with DFT calculations (see Section S2 of the Supporting Information). The average energy gain upon adhesion of the water molecule on the surface at room temperature is 0.41 eV. Once the molecule is anchored in this way, it does not diffuse sizably at room temperature on the nanosecond time scale.

To study water infiltration within the MAPI crystal, we calculated the associated energy gain of placing the water molecule inside the MAPI bulk, ΔE_{in}. We find $\Delta E_{in} = 0.29$ eV at room temperature, meaning that water infiltration is possible, though less convenient than water absorption on the surface. This is consistent with *ab initio* results.[41,42] A comparison between MYP1 and DFT results is reported in Table 1. Further details can be found in the Supporting Information.

Infiltration on a perfect crystal surface is found to be a rare event, indicating the existence of an energy barrier. Water infiltration during NPT dynamics at room temperature was observed only by applying a constant force on water perpendicular to the MAPI surface. This provides a rough estimate of the energy barrier of 0.3−0.5 eV. The existence of an energy barrier was suggested also by *ab initio* calculations,[41] reporting a static barrier between 0.023 and 0.23 eV, depending on the orientation of the MA cations. This is also consistent with results based on CPMD simulations of vapor,[63] in which water infiltration was not observed. In the case of damaged surfaces or in the presence of more than one water molecule (see below), the infiltration process can be faster.

Table 1. Energy Gain (eV/H_2O) for Adhesion and Infiltration of a Single Water Molecule

	energetics				
	0 K				300 K
	MYP1[a]	DFT[a]	DFT[b]	DFT[c]	MYP1[a]
adhesion	0.42	0.71	0.44	0.38−0.54	0.41
infiltration	0.23	0.37	0.45	0.05−0.3	0.29

[a]This work. [b]From ref 42. [c]From ref 41.

Once infiltrated, the molecule spends most of the time vibrating inside the MAPI tetragonal cell containing it. In agreement with ref 42, it is preferentially located on the sides of the perovskite cage, where it can form hydrogen bonds with the I atoms. The distribution of positions of hydrogen and oxygen atoms shows that H spends most of the time in proximity to I atoms, while O stays closer to the positive MA cation, as expected for electrostatic arguments (see, for example, top panel of Figure 3), due to a tendency to form O−H links (see results at $T = 0$ K, Supporting Information).

Diffusion between adjacent cells is observed during long dynamics at room temperature. The molecule can jump from one PbI cage to the neighboring ones of the bulk. As the temperature is raised, the water diffusion increases rapidly, indicating a thermally activated process. An example of diffusion trajectory is reported in Figure 3. By fitting the average mean square displacements (MSD) with the Einstein relation MSD = $6Dt$ we estimated the diffusion coefficients D at different temperatures. At $T = 300$ K a value of $D = 1.7 \times 10^{-8}$ cm^2/s and an activation energy of 0.28 eV are found. Interestingly, this value is comparable with the case of water diffusion in perovskite oxides.[64]

Liquid Phase Analysis. We now focus our attention on the opposite limit, *i.e.*, the MAPI surface in the presence of liquid water (see Figure 2). It is interesting first to calculate the adhesion energy ΔE_{wet} necessary to separate a unit surface of water (wetting layer) from the crystal. An energy gain of 1.45 eV/nm^2 is found, corresponding to 0.23 N/m. As a term of comparison, the interaction energy between water and silica is ∼0.2 N/m.[65] A summary of the water/MAPI energetics is reported in Table 2.

The wettability of the perovskites favors the contact between the water and the surface, making the degradation process possible. Accurate measurements of degradation velocity are not reported in the literature, but available data at room temperature indicate that samples of thickness 1−100 μm degraded in a few seconds.[38] In terms of microscopic quantities this corresponds to a few monolayers (∼1 nm) dissolved in 10^4−10^6 ns. Accordingly, within the time scale typical of molecular dynamics simulations (up to 100 ns in the present study) a sizable degradation at room temperature is not expected. This is in fact the case. However, as the temperature increases, the degradation kinetics rapidly increases. Already at 340 K, degradation events can be observed within 100 ns. At

DOI: 10.1021/acsnano.7b04116
ACS Nano XXXX, XXX, XXX−XXX

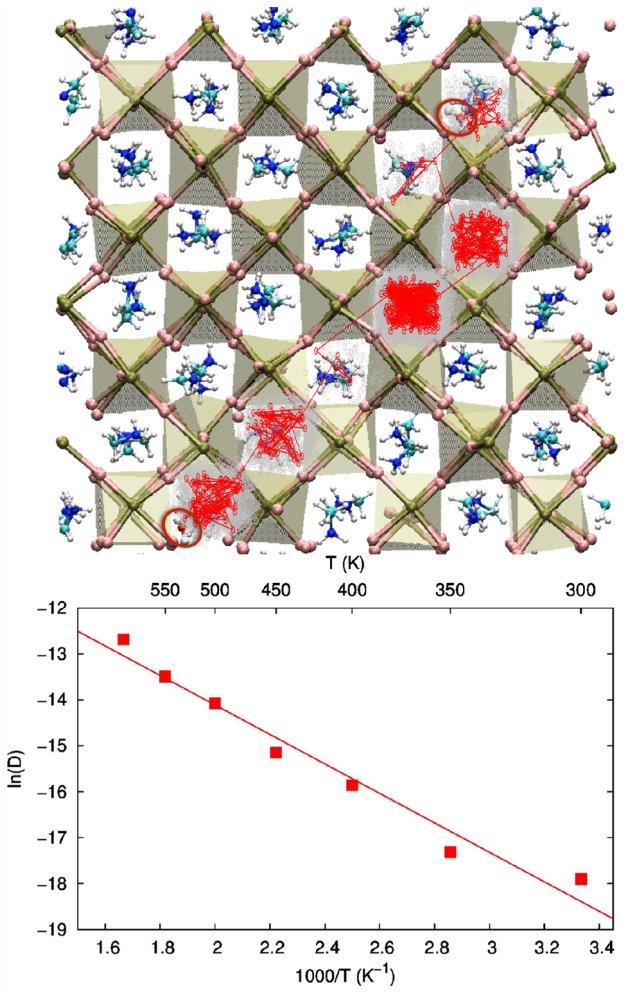

Figure 3. (Top) Illustration of the H_2O diffusion inside a MAPI bulk at T = 550 K during 5 ns. The water molecule jumps from a MAPI cell to an adjacent one in discrete steps. Red (gray) circles represent consecutive positions of oxygen (hydrogen) atoms of water along the trajectory. The initial and final positions of the water molecule are also shown. (Bottom) Arrhenius plot of the diffusion coefficients.

Table 2. Energetics: Energy Gain (ΔE) for Adhesion, Infiltration, and Wetting; Kinetics: First Two Columns Report the Diffusion Coefficient in the Crystal (D) at T = 300 K and Last Two Columns Report the Activation Energy (E_A) for Diffusion and Degradation

Energetics			
		ΔE	
	adhesion	0.41 eV/H_2O	
	infiltration	0.29 eV/H_2O	
	wetting	0.23 N/m	
Kinetics			
	(T = 300 K)	E_A (eV)	
D	1.7 × 10^{-8} cm^2/s	diffusion	0.28
		degradation	0.36

higher temperatures the full degradation of a 4 nm thick crystal was observed during the dynamics. Under the hypothesis that the degradation velocity v follows an Arrhenius dependence on temperature ($v \sim \exp(-E_A/K_BT)$), we plot $\ln(v/l_0)$ *vs* $1000/T$, where l_0 is the thickness of the MAPI monolayer (0.63 nm) and $t_0 = l_0/v$ is the time at which the first layer is completely degraded into PbI_2. The corresponding plot is reported in the bottom panel of Figure 4, and it provides E_A = 0.36 eV. Figure 4 shows some snapshots of the degradation process simulated at T = 480 K: after 4 ns, the first layer has been transformed into PbI_2 by the water, and it takes about 50 ns to degrade the whole slab. The degradation starts locally at some random point of the surface where a Pb−I bond breaks. After that the degradation tends to propagate laterally along the outermost layer of the crystal, and the MAPI is degraded in a layer-by-layer fashion. PbI_2 layers are formed, while MAI is dissolved in water as MA^+ molecules and I^- ions. This is in agreement with experimental results reporting PbI_2 as the product of degradation.[38]

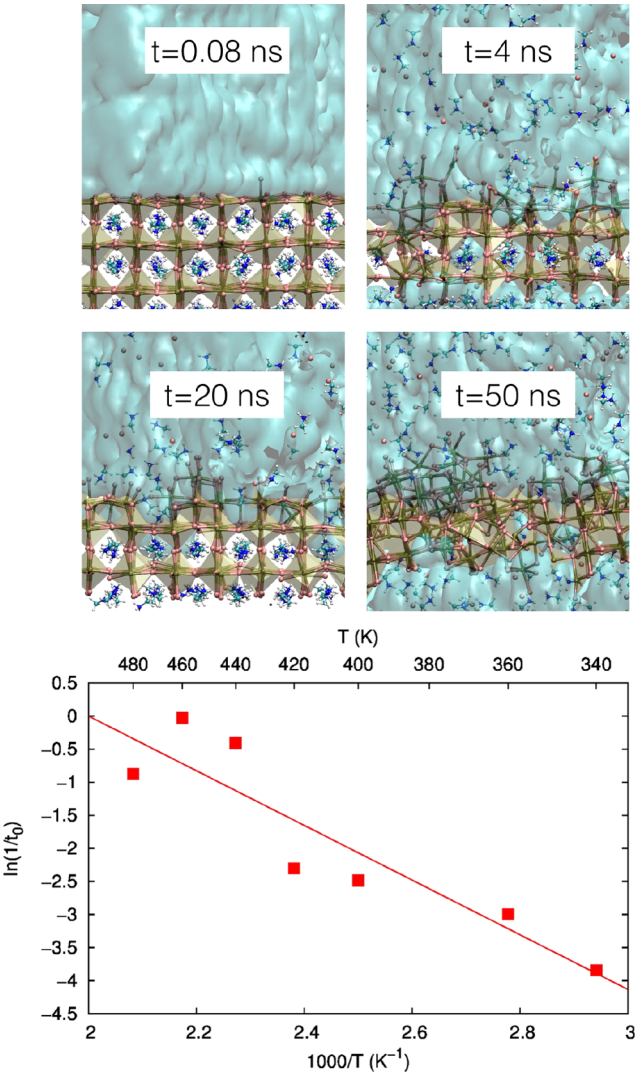

Figure 4. (Top) Snapshots of water degradation by liquid water at T = 480 K. (Bottom) Arrhenius plot for MAPI degradation in liquid water. $t_0 = l_0/v$ is the time (in nanoseconds) at which the first layer is completely transformed into PbI_2.

We have also performed a study of MAPI degradation by starting from the MAI-terminated surface. To limit the computational cost, we have considered only 300 and 480 K. In agreement with the CPMD simulations[42] (reporting the solvation of one MAI unit at room temperature in 8.5 ps) we observe a fast dissolution (within 10 ps) of outermost MAI

DOI: 10.1021/acsnano.7b04116
ACS Nano XXXX, XXX, XXX−XXX

layers (see Figure S4 of the Supporting Information). After the removal of external MAI units the surface evolves into a PbI_2-terminated one. The surface is not perfectly flat due to the presence of an almost half-coverage of I adatoms. At longer simulation time, we observe that the degradation is analogous to the PbI_2 case. Eventually (at 480 K and after ~40 ns of annealing) the MAPI is fully dissolved into insoluble PbI_2 and solvated MA and I ions (see Figure S5 of the Supporting Information).

Past literature has indicated that an important channel for degradation of MAPI either under thermal stress or in the presence of water is the deprotonation of methylammonium. In this case a dependence on the pH of water is expected, but the effect has been found to be modest.[38] Furthermore, the energy cost for deprotonation is high (~1 eV). In the present study we find a lower activation energy mechanism for the spontaneous dissolution of the crystal into its ionic components in water. This fast process can possibly facilitate further decomposition by higher energy and slower fragmentation of methylammonium. As explained below, the dissolution process relies on the ability of water molecules to damage the crystal by a collective action.

Degradation by Collective Molecular Mechanisms. Summarizing the previous results, we have found that the infiltration and diffusion of a single water molecule in a MAPI crystal is possible and does not induce degradation. Conversely, water in the liquid phase is able to irreversibly dissolve the perovskite. It is natural to ask what is the reason for such a different behavior and whether a minimal amount of water exists that is necessary and sufficient to degradate MAPI. In order to answer this question, we consider increasing the amount of water on the MAPI surface, and we study the damage induced on the surface as a function of the number of water molecules on the perovskite surface. We focus on T = 340 K, as a similar analysis at room temperature, though possible, would require much longer simulations and a huge computational cost. We start by covering 10% of the MAPI surface sites by water molecules, and we then increase the coverage up to 100% (*i.e.*, a complete water monolayer). The first degradation event is observed for 75% water coverage, corresponding to a surface density of 5.9×10^{-9} g/cm^2: one I atom is lifted from the surface attracted by the surrounding H_2O molecules (see Figure 5a,b1). A Pb–I bond is thus broken, and two water molecules infiltrate inside the crystal (see Figure 5b2,b3). A network of hydrogen bonds is formed between the water molecules and surface I atoms so as to bring the number of donor hydrogen bonds per molecule toward its ideal value.[66] This is the first step of the water degradation, as detailed in the previous section. It is interesting to compare the degradation energy calculated from the dynamics with the energy cost associated with the formation of I defects on the surface. In the absence of water the formation energy is 0.62 eV. Notably, in the presence of a cluster of four water molecules, this value decreases to 0.26 eV, close to the activation energy of 0.36 eV. This, together with the observation of the mechanism of water intrusion, suggests that the barrier is mainly due to the cost of forming the hydrated I defect. Furthermore, these results show that the presence of aggregated water molecules acts as catalyzer for the formation of such defects and the degradation of MAPI (see Supporting Information, Section S3).

For higher temperatures, this phenomenon is observed at lower water coverages: for example, at T = 480 K a coverage as small as 20% is sufficient to initiate the surface degradation process. We remark here that the Pb–I bond breaking and subsequent multiple water infiltrations are possible only when more than one H_2O molecule is present in the proximity of the bond: in the simulated systems at low coverage, this correspond to having at least three water molecules around the I atom. These results clearly indicate a collective effect of water molecules.

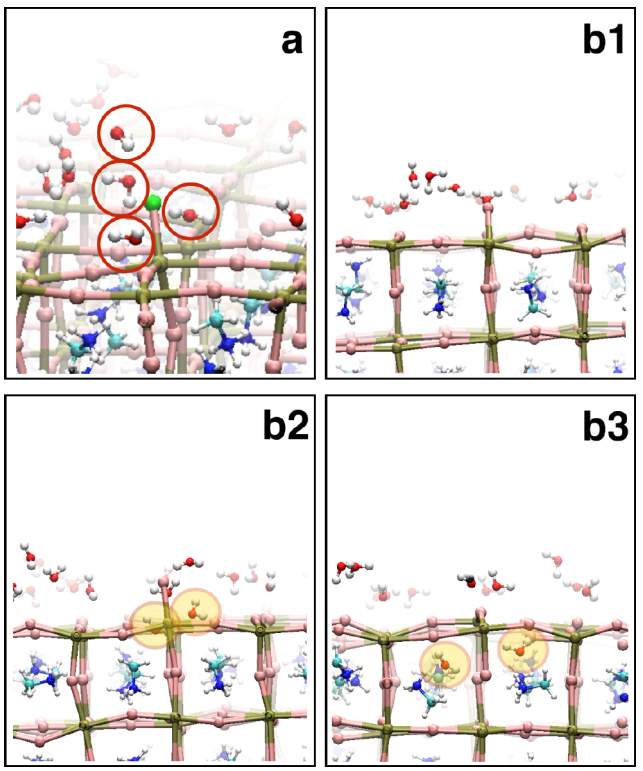

Figure 5. Snapshots taken during the simulation of 75% water coverage on a MAPI surface at T = 340 K. (a) View of three H_2O molecules lifting an I atom (depicted in green for clarity). (b) Subsequent moments of the simulation, showing water infiltration (the yellow circles indicate the infiltrated molecules).

In the vapor phase (containing less than 1 molecule per 10^3 nm^3) water is not able to damage the PbI network, and we can speculate that water progressively infiltrates and diffuses as isolated molecules without damaging the crystal until the formation of the hydrated phase. Conversely, when water is aggregated on the surface, irreversible degradation of the lattice can occur.

CONCLUSIONS

By calibrating a simple force field for water/MAPI we have been able to study the interaction of a MAPI crystal with vapor and to simulate its full dissolution in liquid water. The study provides a comprehensive picture of the transformation phenomena occurring in MAPI in the presence of water. At room temperature the water vapor absorption is energetically favored by 0.29 eV and the infiltrated water molecules can diffuse without damaging the crystal structure, with a diffusion coefficient $D = 1.7 \times 10^{-8}$ cm^2/s at room temperature.

On the contrary the dissolution of MAPI in liquid water is irreversible and thermally activated with a barrier of 0.36 eV. The underlying microscopic mechanism of degradation is explained as a collective action of water molecules that perturb

DOI: 10.1021/acsnano.7b04116
ACS Nano XXXX, XXX, XXX–XXX

the inorganic framework by lifting I atoms, making liquid water infiltration possible. In the presence of bulk water, at the initial stages of the degradation, a tendency of liquid water to transform the material layer by layer is observed, by solvating MA and I ions and producing insoluble PbI_2 films.

By using models at increasing water coverage, we are able to rationalize the transition from the reversible kinetics in the presence of water vapor to the irreversible degradation of the crystal in liquid. In particular, we show that three water molecules are needed to deteriorate locally the perfect PbI-terminated surface of the hybrid perovskite.

We point out that previous theoretical works exploring the picosecond scale were not able to observe PbI_2-surface degradation and concluded that such a surface could act as a protective layer. Here, we show that on a longer nanosecond scale the MAPI degradation is indeed possible also from the PbI_2-terminated surfaces, although it is less favored (*i.e.*, slower) than from MAI-terminated ones. The model developed in the present work and applied to perfect crystalline MAPI is also suitable to study realistic samples containing extended defects and grain boundaries.

COMPUTATIONAL DETAILS

Model potential molecular dynamics simulations were performed by using the LAMMPS code.[67] The MYP1 parameters can be found in the Supporting Information. The long-range electrostatic forces were calculated by the particle−particle particle-mesh Ewald algorithm,[68] and van der Waals interactions were cut off at 10 Å. The velocity-Verlet algorithm[69] with a time step as small as 0.5 fs was used to solve the equations of motion. Trajectories were analyzed by using the VMD 1.9 code.[70] After a conjugate gradient minimization and a short (5 ps) low-temperature (1 K) relaxation, the systems were heated to the temperatures of interest. Temperature was controlled by a Nose-Hoover thermostat.[71,72] Simulations in liquid water were run for up to 50 ns. To estimate the diffusion coefficients for absorbed water molecules, we performed 10 independent simulations for each temperature, and we averaged the molecule MSD.

DFT calculations were performed by the plane-wave Quantum ESPRESSO code[73] with the LDA exchange−correlation functional, ultrasoft-pseudopotentials for all atomic species, 45 Ry kinetic energy cutoff for the orbital and 300 Ry for charge density, and 4 × 4 × 1 Monkhorst−Pack reciprocal space sampling.

ASSOCIATED CONTENT

Supporting Information

The Supporting Information is available free of charge on the ACS Publications website at DOI: 10.1021/acsnano.7b04116.

MYP1 potential parameters for MAPI and water−MAPI systems, model validation for MAPI and PbI_2; water−MAPI model validation against *ab initio* data for water infiltration and adhesion; room-temperature dynamics of water/PbI_2 crystal interface and solvated PbI_2 trimer; MAPI degradation from MAI-terminated surface; formation energy of iodine point-defects on PbI_2-terminated MAPI surface (PDF)

AUTHOR INFORMATION

Corresponding Authors

*E-mail: caddeo@iom.cnr.it.

*E-mail: mattoni@iom.cnr.it.

ORCID

Claudia Caddeo: 0000-0002-1090-9897

Alessio Filippetti: 0000-0002-9144-7005

Alessandro Mattoni: 0000-0002-1381-6557

Notes

The authors declare no competing financial interest.

ACKNOWLEDGMENTS

We acknowledge financial support by MIUR through Project PON 04A2_0490 M2M NETERGIT and computational support from CINECA through ISCRA (projects THESTA, THEHYPE, MYPALLOY) and PRACE initiatives (project UNWRAP) and from CRS4 Computing Center (Piscina Manna, Pula, Italy).

REFERENCES

(1) Mattoni, A.; Filippetti, A.; Caddeo, C. Modeling Hybrid Perovskites by Molecular Dynamics. *J. Phys.: Condens. Matter* **2017**, *29*, 043001.

(2) Mitzi, D. B. *Progress in Inorganic Chemistry*; John Wiley and Sons, Inc., 2007; pp 1−121.

(3) Stoumpos, C. C.; Malliakas, C. D.; Kanatzidis, M. G. Semiconducting Tin and Lead Iodide Perovskites with Organic Cations: Phase Transitions, High Mobilities, and Near-Infrared Photoluminescent Properties. *Inorg. Chem.* **2013**, *52*, 9019−9038.

(4) Yin, W.-J.; Yang, J.-H.; Kang, J.; Yan, Y.; Wei, S.-H. Halide Perovskite Materials for Solar Cells: a Theoretical Review. *J. Mater. Chem. A* **2015**, *3*, 8926−8942.

(5) Burschka, J.; Pellet, N.; Moon, S.-J.; Humphry-Baker, R.; Gao, P.; Nazeeruddin, M. K.; Gratzel, M. Sequential Deposition as a Route to High-Performance Perovskite-Sensitized Solar Cells. *Nature* **2013**, *499*, 316−319.

(6) Egger, D. A.; Rappe, A. M.; Kronik, L. Hybrid Organic-Inorganic Perovskites on the Move. *Acc. Chem. Res.* **2016**, *49*, 573−581.

(7) Polman, A.; Knight, M.; Garnett, E. C.; Ehrler, B.; Sinke, W. C. Photovoltaic Materials: Present Efficiencies and Future Challenges. *Science (Washington, DC, U. S.)* **2016**, *352*, aad4424−aad4424.

(8) Ha, S. T.; Liu, X.; Zhang, Q.; Giovanni, D.; Sum, T. C.; Xiong, Q. Synthesis of Organic-Inorganic Lead Halide Perovskite Nanoplatelets: Towards High-Performance Perovskite Solar Cells and Optoelectronic Devices. *Adv. Opt. Mater.* **2014**, *2*, 838−844.

(9) Yakunin, S.; Sytnyk, M.; Kriegner, D.; Shrestha, S.; Richter, M.; Matt, G. J.; Azimi, H.; Brabec, C. J.; Stangl, J.; Kovalenko, M. V.; Heiss, W. Detection of X-ray Photons by Solution-Processed Lead Halide Perovskites. *Nat. Photonics* **2015**, *9*, 444−449.

(10) Zhang, Q.; Ha, S. T.; Liu, X.; Sum, T. C.; Xiong, Q. Room-Temperature Near-Infrared High-Q Perovskite Whispering-Gallery Planar Nanolasers. *Nano Lett.* **2014**, *14*, 5995−6001.

(11) Zhu, H.; Fu, Y.; Meng, F.; Wu, X.; Gong, Z.; Ding, Q.; Gustafsson, M. V.; Trinh, M. T.; Jin, S.; Zhu, X.-Y. Lead Halide Perovskite Nanowire Lasers with Low Lasing Thresholds and High Quality Factors. *Nat. Mater.* **2015**, *14*, 636−642.

(12) Bokdam, M.; Sander, T.; Stroppa, A.; Picozzi, S.; Sarma, D. D.; Franchini, C.; Kresse, G. Role of Polar Phonons in the Photo Excited State of Metal Halide Perovskites. *Sci. Rep.* **2016**, *6*, 28618.

(13) Park, S.; Chang, W. J.; Lee, C. W.; Park, S.; Ahn, H.-Y.; Nam, K. T. Photocatalytic Hydrogen Generation from Hydriodic Acid Using Methylammonium Lead Iodide in Dynamic Equilibrium with Aqueous Solution. *Nat. Energy* **2016**, *2*, 16185.

(14) Filippetti, A.; Caddeo, C.; Delugas, P.; Mattoni, A. Appealing Perspectives of Hybrid Lead Iodide Perovskites as Thermoelectric Materials. *J. Phys. Chem. C* **2016**, *120*, 28472−28479.

(15) Lee, C.; Hong, J.; Stroppa, A.; Whangbo, M.-H.; Shim, J. H. Organic-Inorganic Hybrid Perovskites ABI3 (A = CH3NH3, NH2CHNH2; B = Sn, Pb) as Potential Thermoelectric Materials: a Density Functional Evaluation. *RSC Adv.* **2015**, *5*, 78701−78707.

(16) Filippetti, A.; Mattoni, A.; Caddeo, C.; Saba, M. I.; Delugas, P. Low Electron-Polar Optical Phonon Scattering as a Fundamental Aspect of Carrier Mobility in Methylammonium Lead Halide

DOI: 10.1021/acsnano.7b04116
ACS Nano XXXX, XXX, XXX−XXX

CH3NH3PbI3 Perovskites. *Phys. Chem. Chem. Phys.* **2016**, *18*, 15352−15362.
(17) Dualeh, A.; Gao, P.; Seok, S. I.; Nazeeruddin, M. K.; Grätzel, M. Thermal Behavior of Methylammonium Lead-Trihalide Perovskite Photovoltaic Light Harvesters. *Chem. Mater.* **2014**, *26*, 6160−6164.
(18) Eperon, G. E.; Stranks, S. D.; Menelaou, C.; Johnston, M. B.; Herz, L. M.; Snaith, H. J. Formamidinium Lead Trihalide: a Broadly Tunable Perovskite for Efficient Planar Heterojunction Solar Cells. *Energy Environ. Sci.* **2014**, *7*, 982−988.
(19) Stranks, S. D.; Snaith, H. J. Metal-halide Perovskites For Photovoltaic and Light-Emitting Devices. *Nat. Nanotechnol.* **2015**, *10*, 391−402.
(20) Frost, J. M.; Butler, K. T.; Brivio, F.; Hendon, C. H.; van Schilfgaarde, M.; Walsh, A. Atomistic Origins of High-Performance in Hybrid Halide Perovskite Solar Cells. *Nano Lett.* **2014**, *14*, 2584−2590.
(21) Niu, G.; Li, W.; Meng, F.; Wang, L.; Dong, H.; Qiu, Y. Study on the Stability of CH3NH3PbI3 Films and the Effect of Post-Modification by Aluminum Oxide in All-Solid-State Hybrid Solar Cells. *J. Mater. Chem. A* **2014**, *2*, 705−710.
(22) Yang, J.; Siempelkamp, B. D.; Liu, D.; Kelly, T. L. Investigation of CH3NH3PbI3 Degradation Rates and Mechanisms in Controlled Humidity Environments Using *in Situ* Techniques. *ACS Nano* **2015**, *9*, 1955−1963.
(23) Christians, J. A.; Herrera, P. A. M.; Kamat, P. V. Transformation of the Excited State and Photovoltaic Efficiency of CH3NH3PbI3 Perovskite upon Controlled Exposure to Humidified Air. *J. Am. Chem. Soc.* **2015**, *137*, 1530−1538.
(24) Han, Y.; Meyer, S.; Dkhissi, Y.; Weber, K.; Pringle, J. M.; Bach, U.; Spiccia, L.; Cheng, Y.-B. Degradation Observations of Encapsulated Planar CH3NH3PbI3 Perovskite Solar Cells at High Temperatures and Humidity. *J. Mater. Chem. A* **2015**, *3*, 8139−8147.
(25) Kang, S. M.; Ahn, N.; Lee, J.-W.; Choi, M.; Park, N.-G. Water-Repellent Perovskite Solar Cell. *J. Mater. Chem. A* **2014**, *2*, 20017−20021.
(26) Jung, H. S.; Park, N.-G. Perovskite Solar Cells: From Materials to Devices. *Small* **2015**, *11*, 10−25.
(27) Hwang, I.; Jeong, I.; Lee, J.; Ko, M. J.; Yong, K. Enhancing Stability of Perovskite Solar Cells to Moisture by the Facile Hydrophobic Passivation. *ACS Appl. Mater. Interfaces* **2015**, *7*, 17330−17336.
(28) Eperon, G. E.; Burlakov, V. M.; Docampo, P.; Goriely, A.; Snaith, H. J. Morphological Control for High Performance, Solution-Processed Planar Heterojunction Perovskite Solar Cells. *Adv. Funct. Mater.* **2014**, *24*, 151−157.
(29) Kim, I. S.; Cao, D. H.; Buchholz, D. B.; Emery, J. D.; Farha, O. K.; Hupp, J. T.; Kanatzidis, M. G.; Martinson, A. B. F. Liquid Water- and Heat-Resistant Hybrid Perovskite Photovoltaics *via* an Inverted ALD Oxide Electron Extraction Layer Design. *Nano Lett.* **2016**, *16*, 7786−7790.
(30) Xie, F. X.; Zhang, D.; Su, H.; Ren, X.; Wong, K. S.; Grätzel, M.; Choy, W. C. H. Vacuum-Assisted Thermal Annealing of CH3NH3PbI3 for Highly Stable and Efficient Perovskite Solar Cells. *ACS Nano* **2015**, *9*, 639−646.
(31) Bass, K. K.; McAnally, R. E.; Zhou, S.; Djurovich, P. I.; Thompson, M. E.; Melot, B. C. Influence of Moisture on the Preparation, Crystal Structure, and Photophysical Properties of Organohalide Perovskites. *Chem. Commun.* **2014**, *50*, 15819−15822.
(32) Zhou, H.; Chen, Q.; Li, G.; Luo, S.; Song, T.-b.; Duan, H.-S.; Hong, Z.; You, J.; Liu, Y.; Yang, Y. Interface Engineering of Highly Efficient Perovskite Solar Cells. *Science* **2014**, *345*, 542−546.
(33) Li, B.; Fei, C.; Zheng, K.; Qu, X.; Pullerits, T.; Cao, G.; Tian, J. Constructing Water-Resistant CH3NH3PbI3 Perovskite Films *via* Coordination Interaction. *J. Mater. Chem. A* **2016**, *4*, 17018−17024.
(34) Saliba, M.; Matsui, T.; Domanski, K.; Seo, J.-Y.; Ummadisingu, A.; Zakeeruddin, S. M.; Correa-Baena, J.-P.; Tress, W. R.; Abate, A.; Hagfeldt, A.; Gratzel, M. Incorporation of Rubidium Cations into Perovskite Solar Cells Improves Photovoltaic Performance. *Science (Washington, DC, U. S.)* **2016**, *354*, 206−209.
(35) Leguy, A. M. A.; Hu, Y.; Campoy-Quiles, M.; Alonso, M. I.; Weber, O. J.; Azarhoosh, P.; van Schilfgaarde, M.; Weller, M. T.; Bein, T.; Nelson, J.; Docampo, P.; Barnes, P. R. F. Reversible Hydration of CH3NH3PbI3 in Films, Single Crystals, and Solar Cells. *Chem. Mater.* **2015**, *27*, 3397−3407.
(36) Müller, C.; Glaser, T.; Plogmeyer, M.; Sendner, M.; Döring, S.; Bakulin, A. A.; Brzuska, C.; Scheer, R.; Pshenichnikov, M. S.; Kowalsky, W.; Pucci, A.; Lovrinčić, R. Water Infiltration in Methylammonium Lead Iodide Perovskite: Fast and Inconspicuous. *Chem. Mater.* **2015**, *27*, 7835−7841.
(37) Zhu, Z.; Hadjiev, V. G.; Rong, Y.; Guo, R.; Cao, B.; Tang, Z.; Qin, F.; Li, Y.; Wang, Y.; Hao, F.; Venkatesan, S.; Li, W.; Baldelli, S.; Guloy, A. M.; Fang, H.; Hu, Y.; Yao, Y.; Wang, Z.; Bao, J. Interaction of Organic Cation with Water Molecule in Perovskite MAPbI3: From Dynamic Orientational Disorder to Hydrogen Bonding. *Chem. Mater.* **2016**, *28*, 7385−7393.
(38) Hailegnaw, B.; Kirmayer, S.; Edri, E.; Hodes, G.; Cahen, D. Rain on Methylammonium Lead Iodide Based Perovskites: Possible Environmental Effects of Perovskite Solar Cells. *J. Phys. Chem. Lett.* **2015**, *6*, 1543−1547.
(39) Smecca, E.; Numata, Y.; Deretzis, I.; Pellegrino, G.; Boninelli, S.; Miyasaka, T.; La Magna, A.; Alberti, A. Stability of Solution-Processed MAPbI3 and FAPbI3 Layers. *Phys. Chem. Chem. Phys.* **2016**, *18*, 13413−13422.
(40) Tong, C.-J.; Geng, W.; Tang, Z.-K.; Yam, C.-Y.; Fan, X.-L.; Liu, J.; Lau, W.-M.; Liu, L.-M. Uncovering the Veil of the Degradation in Perovskite CH3NH3PbI3 upon Humidity Exposure: A First-Principles Study. *J. Phys. Chem. Lett.* **2015**, *6*, 3289−3295.
(41) Koocher, N. Z.; Saldana-Greco, D.; Wang, F.; Liu, S.; Rappe, A. M. Polarization Dependence of Water Adsorption to CH3NH3PbI3 (001) Surfaces. *J. Phys. Chem. Lett.* **2015**, *6*, 4371−4378.
(42) Mosconi, E.; Azpiroz, J. M.; De Angelis, F. *Ab Initio* Molecular Dynamics Simulations of Methylammonium Lead Iodide Perovskite Degradation by Water. *Chem. Mater.* **2015**, *27*, 4885−4892.
(43) Long, R.; Fang, W.; Prezhdo, O. V. Moderate Humidity Delays Electron-Hole Recombination in Hybrid Organic-Inorganic Perovskites: Time-Domain *Ab Initio* Simulations Rationalize Experiments. *J. Phys. Chem. Lett.* **2016**, *7*, 3215−3222.
(44) Car, R.; Parrinello, M. Unified Approach for Molecular Dynamics and Density-Functional Theory. *Phys. Rev. Lett.* **1985**, *55*, 2471−2474.
(45) Mattoni, A.; Filippetti, A.; Saba, M. I.; Delugas, P. Methylammonium Rotational Dynamics in Lead Halide Perovskite by Classical Molecular Dynamics: The Role of Temperature. *J. Phys. Chem. C* **2015**, *119*, 17421−17428.
(46) Hata, T.; Giorgi, G.; Yamashita, K. The Effects of the Organic−Inorganic Interactions on the Thermal Transport Properties of CH3NH3PbI3. *Nano Lett.* **2016**, *16*, 2749−2753.
(47) Qian, X.; Gu, X.; Yang, R. Lattice Thermal Conductivity of Organic-Inorganic Hybrid Perovskite CH3NH3PbI3. *Appl. Phys. Lett.* **2016**, *108*, 063902.
(48) Mattoni, A.; Filippetti, A.; Saba, M.; Caddeo, C.; Delugas, P. Temperature Evolution of Methylammonium Trihalide Vibrations at the Atomic Scale. *J. Phys. Chem. Lett.* **2016**, *7*, 529−535.
(49) Delugas, P.; Caddeo, C.; Filippetti, A.; Mattoni, A. Thermally Activated Point-Defects Diffusion in Methylammonium Lead Trihalide: Anisotropic and Ultra-High Mobility of Iodine. *J. Phys. Chem. Lett.* **2016**, *13*, 2356−2361.
(50) Caddeo, C.; Melis, C.; Saba, M. I.; Filippetti, A.; Colombo, L.; Mattoni, A. Tuning the Thermal Conductivity of Methylammonium Lead Halide by the Molecular Substructure. *Phys. Chem. Chem. Phys.* **2016**, *18*, 24318−24324.
(51) Wang, M.; Lin, S. Anisotropic and Ultralow Phonon Thermal Transport in Organic-Inorganic Hybrid Perovskites: Atomistic Insights into Solar Cell Thermal Management and Thermoelectric Energy Conversion Efficiency. *Adv. Funct. Mater.* **2016**, *26*, 5297−5306.
(52) Dar, M. I.; Jacopin, G.; Meloni, S.; Mattoni, A.; Arora, N.; Boziki, A.; Zakeeruddin, S. M.; Rothlisberger, U.; Grätzel, M. Origin of Unusual Bandgap Shift and Dual Emission in Organic-Inorganic Lead

DOI: 10.1021/acsnano.7b04116
ACS Nano XXXX, XXX, XXX−XXX

Halide Perovskites. *Sci. Adv.* **2016**, *2*, e160115610.1126/sciadv.1601156.
(53) Gutierrez-Sevillano, J. J.; Ahmad, S.; Calero, S.; Anta, J. A. Molecular Dynamics Simulations of Organohalide Perovskite Precursors: Solvent Effects in the Formation of Perovskite Solar Cells. *Phys. Chem. Chem. Phys.* **2015**, *17*, 22770−22777.
(54) Horinek, D.; Mamatkulov, S. I.; Netz, R. R. Rational Design of Ion Force Fields Based on Thermodynamic Solvation Properties. *J. Chem. Phys.* **2009**, *130*, 124507.
(55) de Araujo, A. S.; Sonoda, M. T.; Piro, O. E.; Castellano, E. E. Development of New Cd2+ and Pb2+ Lennard-Jones Parameters for Liquid Simulations. *J. Phys. Chem. B* **2007**, *111*, 2219−2224.
(56) Delugas, P.; Filippetti, A.; Mattoni, A. Methylammonium Fragmentation in Amines as Source of Localized Trap Levels and the Healing Role of Cl in Hybrid Lead-Iodide Perovskites. *Phys. Rev. B: Condens. Matter Mater. Phys.* **2015**, *92*, 045301.
(57) Juarez-Perez, E. J.; Hawash, Z.; Raga, S. R.; Ono, L. K.; Qi, Y. Thermal Degradation of CH3NH3PbI3 Perovskite into NH3 and CH3I Gases Observed by Coupled Thermogravimetry-Mass Spectrometry Analysis. *Energy Environ. Sci.* **2016**, *9*, 3406−3410.
(58) Haruyama, J.; Sodeyama, K.; Han, L.; Tateyama, Y. Termination Dependence of Tetragonal CH3NH3PbI3 Surfaces for Perovskite Solar Cells. *J. Phys. Chem. Lett.* **2014**, *5*, 2903−2909.
(59) Haruyama, J.; Sodeyama, K.; Han, L.; Tateyama, Y. Surface Properties of CH3NH3PbI3 for Perovskite Solar Cells. *Acc. Chem. Res.* **2016**, *49*, 554−561.
(60) Winkler, B.; Dove, M. T.; Salje, E. K. H.; Leslie, M.; Palosz, B. Phonon Stabilized Polytypism in PbI 2: *In Situ* Raman Spectroscopy and Transferable Core-Shell Model Calculations. *J. Phys.: Condens. Matter* **1991**, *3*, 539−550.
(61) Handley, C. M.; Freeman, C. L. A New Potential for Methylammonium Lead Iodide. *Phys. Chem. Chem. Phys.* **2016**, *19*, 2313−2321.
(62) Jorgensen, W. L.; Chandrasekhar, J.; Madura, J. D.; Impey, R. W.; Klein, M. L. Comparison of Simple Potential Functions for Simulating Liquid Water. *J. Chem. Phys.* **1983**, *79*, 926−935.
(63) Zhang, L.; Ju, M.-G.; Liang, W. The Effect of Moisture on the Structures and Properties of Lead Halide Perovskites: a First-Principles Theoretical Investigation. *Phys. Chem. Chem. Phys.* **2016**, *18*, 23174−23183.
(64) Animitsa, I.; Neiman, A.; Kochetova, N.; Korona, D.; Sharafutdinov, A. Chemical Diffusion of Water in the Double Perovskites Ba4Ca2Nb2O11 and Sr6Ta2O11. *Solid State Ionics* **2006**, *177*, 2363−2368. Solid State Ionics 15: Proceedings of the 15th International Conference on Solid State Ionics, Part {II}.
(65) Lee, S. H.; Rossky, P. J. A Comparison of the Structure and Dynamics of Liquid Water at Hydrophobic and Hydrophilic Surfaces: a Molecular Dynamics Simulation Study. *J. Chem. Phys.* **1994**, *100*, 3334−3345.
(66) Jorgensen, W. L.; Madura, J. D. Temperature and Size Dependence for Monte Carlo Simulations of TIP4P Water. *Mol. Phys.* **1985**, *56*, 1381−1392.
(67) Plimpton, S. Fast Parallel Algorithms for Short-Range Molecular Dynamics. *J. Comput. Phys.* **1995**, *117*, 1−19.
(68) Swope, W. C.; Andersen, H. C.; Berens, P. H.; Wilson, K. R. A Computer Simulation Method for the Calculation of Equilibrium Constants for the Formation of Physical Clusters of Molecules: Application to Small Water Clusters. *J. Chem. Phys.* **1982**, *76*, 637−649.
(69) Verlet, L. Computer Experiments on Classical Fluids. I. Thermodynamical Properties of Lennard-Jones Molecules. *Phys. Rev.* **1967**, *159*, 98−103.
(70) Humphrey, W.; Dalke, A.; Schulten, K. VMD: Visual Molecular Dynamics. *J. Mol. Graphics* **1996**, *14*, 33−38.
(71) Nosé, S. A Unified Formulation of the Constant Temperature Molecular Dynamics Methods. *J. Chem. Phys.* **1984**, *81*, 511−519.
(72) Hoover, W. G. Canonical Dynamics: Equilibrium Phase-Space Distributions. *Phys. Rev. A: At., Mol., Opt. Phys.* **1985**, *31*, 1695−1697.
(73) Giannozzi, P.; Baroni, S.; Bonini, N.; Calandra, M.; Car, R.; Cavazzoni, C.; Ceresoli, D.; Chiarotti, G. L.; Cococcioni, M.; Dabo, I.; Dal Corso, A.; de Gironcoli, S.; Fabris, S.; Fratesi, G.; Gebauer, R.; Gerstmann, U.; Gougoussis, C.; Kokalj, A.; Lazzeri, M.; Martin-Samos, L.; et al. QUANTUM ESPRESSO: a Modular and Open-Source Software Project for Quantum Simulations of Materials. *J. Phys.: Condens. Matter* **2009**, *21*, 395502.

DOI: 10.1021/acsnano.7b04116
ACS Nano XXXX, XXX, XXX−XXX